Molecular level characterization of supraglacial dissolved and water extractable organic matter along a hydrological flow path in a Greenland Ice Sheet micro-catchment

Eva L. Doting[1,2,*], Ian T. Stevens[1], Anne M. Kellerman[3], Pamela E. Rossel[4], Runa Antony[4,5], Amy M. McKenna[6, 7], Martyn Tranter[1], Liane G. Benning[4, 8], Robert G. M. Spencer[3], Jon R. Hawkings[2, 9] and Alexandre M. Anesio[1]

[1] Department of Environmental Science, iClimate, Aarhus University, Frederiksborgvej 399, 4000 Roskilde, Denmark
[2] Department of Earth and Environmental Science, University of Pennsylvania, Philadelphia, PA, USA
[3] National High Magnetic Field Laboratory Geochemistry Group and Department of Earth, Ocean, and Atmospheric Science, Florida State University, Tallahassee, FL, USA
[4] Interface Geochemistry Section, German Research Centre for Geosciences, GFZ Potsdam, Telegrafenberg, 14473 Potsdam, Germany
[5] National Centre for Polar and Ocean Research, Ministry of Earth Sciences, Goa, India
[6] National High Magnetic Field Laboratory, Florida State University, Tallahassee, Florida, 32310-4005, USA
[7] Department of Soil and Crop Sciences, Colorado State University, Fort Collins, CO, 80523, USA
[8] Department of Earth Science, Freie Universität Berlin, 12249 Berlin, Germany
[9] iC3, Department of Geosciences, UiT The Arctic University of Norway, Tromsø, Norway

Correspondence to: Eva L. Doting (edoting@sas.upenn.edu)

Abstract.

Sunlight penetrates the bare ice surface of glaciers and ice sheets, giving rise to the presence of a three-dimensional porous matrix of partially melted ice crystals known as the weathering crust. Surface meltwater slowly percolates through this weathering crust, which hosts active and diverse bacterial communities, until it reaches a supraglacial stream. Despite the potential implications of weathering crust dynamics for glacial melting and the export of carbon and nutrients to downstream ecosystems, its role in biogeochemical cycling remains unknown. Here, we use Fourier transform cyclotron resonance mass spectrometry to characterize dissolved organic matter (DOM) along a meltwater flow path in a hydrologically connected micro-catchment on the Southern Greenland Ice Sheet. We find a decrease in the relative abundance of aromatic formulae from surface ice (24.9 ± 2.8%) to weathering crust meltwater (3.5 ± 0.3%) to supraglacial stream water (2.2 ± 0.2%), pointing towards photodegradation of aromatic DOM during supraglacial meltwater transit. The relative abundance of aliphatic and peptide-like formulae in supraglacial stream DOM was lower (38.5 ± 4.0%) than in weathering crust meltwater DOM (50.3 ± 2.4%), likely as a result of microbial respiration of labile compounds within the weathering crust. Hence, we conclude that the weathering crust plays a thus far unexplored role in supraglacial biogeochemical cycling. In addition, we characterize water extractable organic matter isolated from surface ice particulate matter, which was predominantly (61.6 ± 8.1% relative abundance) comprised of aliphatic and peptide-like formulae, providing the first direct evidence of surface ice particulate matter as a potential source of biolabile DOM. As the spatial extent of bare ice surfaces and the associated weathering crust

photic zone is set to increase under a warming climate, our findings underscore the pressing need to further evaluate the role of the weathering crust in supraglacial biogeochemical processes. An understanding of weathering crust biogeochemical cycling is especially critical as climatic warming is predicted to lead to an increase in Arctic rainfall, consequently increasing the frequency of weathering crust degradation events, with unknown impacts on the export of supraglacial DOM to downstream ecosystems.

1 Introduction

During the boreal summer months, 200,000 km^2 of bare ice is exposed on the Greenland Ice Sheet (Ryan et al., 2019). This bare-ice area becomes a hydrologically active drainage system. Meltwater flows through the interfluve weathering crust, a three-dimensional porous matrix of partially melted ice crystals formed by solar radiation penetrating the bare ice surface (Cook et al., 2015; Stevens et al., 2018), before entering supraglacial channels. These channels terminate in supraglacial lakes (Arnold et al., 2014) or enter the en- and sub-glacial hydrological system via moulins or crevasses (Steger et al., 2017), ultimately transferring meltwater to proglacial riverine, lacustrine, and marine environments (Chu, 2014).

This meltwater pathway provides an avenue to deliver dissolved organic matter (DOM) from glacial systems to downstream ecosystems (Hood et al., 2009; Lawson et al., 2014a; Singer et al., 2012). The biolabile and aliphatic-rich character of glacial DOM has been linked to microbial activity on melting bare ice surfaces (Kellerman et al., 2021; Lawson et al., 2014b; Musilova et al., 2017), which can become colonized by algae, bacteria, viruses and fungi (Anesio et al., 2017). Atmospheric deposition can deliver soil or combustion-derived organic matter to glacier surfaces (Bardgett et al., 2007; Barker et al., 2009; Bhatia et al., 2010; Fellman et al., 2015; Holt et al., 2023; Hood et al., 2009; Li et al., 2018; Price et al., 2009; Singer et al., 2012; Spencer et al., 2014; Stubbins et al., 2012), presenting a source of more recalcitrant DOM. However, recently it was shown that photodegradation of such recalcitrant allochthonous DOM can produce aliphatic-rich DOM (Holt et al., 2021), meaning that allochthonous DOM may also contribute to the biolabile character of DOM on glacier surfaces, which receive high amounts of solar radiation during the melt season. While microbial and depositional sources of supraglacial DOM have been inferred from the characterization of DOM in supraglacial streams and laboratory experiments, respectively, an assessment of DOM associated with surface ice, surface ice particulate matter (an admixture of microbes, mineral dust (Simonsen et al., 2019), and atmospherically deposited material), and weathering crust meltwater is currently lacking.

Understanding the role of bare ice surfaces and the associated weathering crust in supraglacial DOM cycling is particularly relevant as climatic warming is projected to increase both the duration of the ice melt season and melt intensity (Rounce et al., 2023), driving an inherent increase in the spatial extent of the weathering crust over the coming decades (Stevens et al., 2022). Furthermore, climatic warming is predicted to cause a wetter Arctic (Dou et al., 2022; Niwano et al., 2021), consequently

increasing the frequency of weathering crust degradation events (Müller and Keeler, 1969). This is likely to affect supraglacial DOM cycling as meltwater pathways and residence periods alter under a changing climate. Notably, the weathering crust hosts an active (Christner, 2018), unique bacterial community (in contrast to snow, the bare-ice surface, and supraglacial streams (Rassner et al., 2024)), which paired with the availability of time (interstitial water velocity is ~ 10^{-2} m d^{-1}, (Irvine-Fynn et al., 2021; Stevens et al., 2018; Yang et al., 2018)), provides a hitherto unexplored environment with the potential to impact supraglacial DOM cycling.

Here, we employ negative electrospray ionization 21 Tesla Fourier transform ion cyclotron resonance mass spectrometry (21 T FT-ICR MS) to characterize DOM along a hydrological flow path from surface ice to weathering crust meltwater to supraglacial stream water in a hydrologically connected micro-catchment on the Southern Greenland Ice Sheet. In addition, we characterize water-extractable organic matter (WEOM) isolated from surface ice particulate matter to approximate the composition of DOM sourced from surface ice particulates. This study aimed to determine if the weathering crust plays a role in supraglacial cycling, and to evaluate the contributions of surface ice particulate matter to the supraglacial DOM pool.

2 Methods

2.1 Site description, near-surface hydrology and sample collection

A ~100 m^2 supraglacial catchment on the southern Greenland Ice Sheet (61° 06' N, 46° 51' W; Fig. 1), located ~1 km from the QAS_M PROMICE weather station (Fausto et al., 2021), was sampled on July 28, 2021 (Day of Year (DOY) 209). Within the catchment, five, 14 cm diameter, auger holes were drilled at 7:00 on DOY 209 (see Fig. 1ii) to measure recharge rate and water table. These holes were drained of water and re-used every two hours between 7:00 and 21:00, with a supplementary measurement at 14:00, using logging ultrasonic range finders. The discharge of the supraglacial stream was measured at the same time intervals at point 'Q' (Fig. 1). Hydraulic conductivity was calculated and water table height interpreted following Stevens et al. (2018), as detailed in the supplementary methods. Weathering crust meltwater flow direction and magnitude were modelled using an uncrewed aerial vehicle (UAV)-derived orthophoto, a digital surface model (DSM; see Fig. S1) and the Spatial Analyst package in ArcMap 10.8 (esri, USA), designed for terrestrial groundwater systems.

Samples for DOC concentration measurements and molecular level characterization of DOM and WEOM were collected at 14:00 local time. Surface ice (SI in Fig. 1ii; n = 4) was collected from areas with visible presence of surficial particulate matter using a sample-cleaned ice axe to scrape the top ~2 cm of ice into acid cleaned (1.2 M HCl) 1 L polycarbonate bottles. Ice was melted in the dark and filtered over combusted glass fibre filters (47 mm, 0.7 μm GF/F filter, Whatman). The surface ice particulate matter retained on the filter was collected into 150 mL acid-cleaned polycarbonate bottles and stored in the dark at -20 °C until isolation of WEOM. Surface ice filtrates were acidified (pH 2, HCl) and aliquots for DOC concentration analysis were stored in furnaced 40 mL amber vials with acid-washed caps and PTFE-lined septa in the dark at 4 °C. The remainder of

the acidified sample was stored in the dark in an acid cleaned polycarbonate bottle until solid phase extraction at GFZ Potsdam, Germany. Four replicates of weathering crust meltwater were collected from auger hole D (see Fig. 1ii), and five replicates of supraglacial stream water at point 'Q' were collected into 1 L polycarbonate bottles and processed as per the surface ice filtrate.

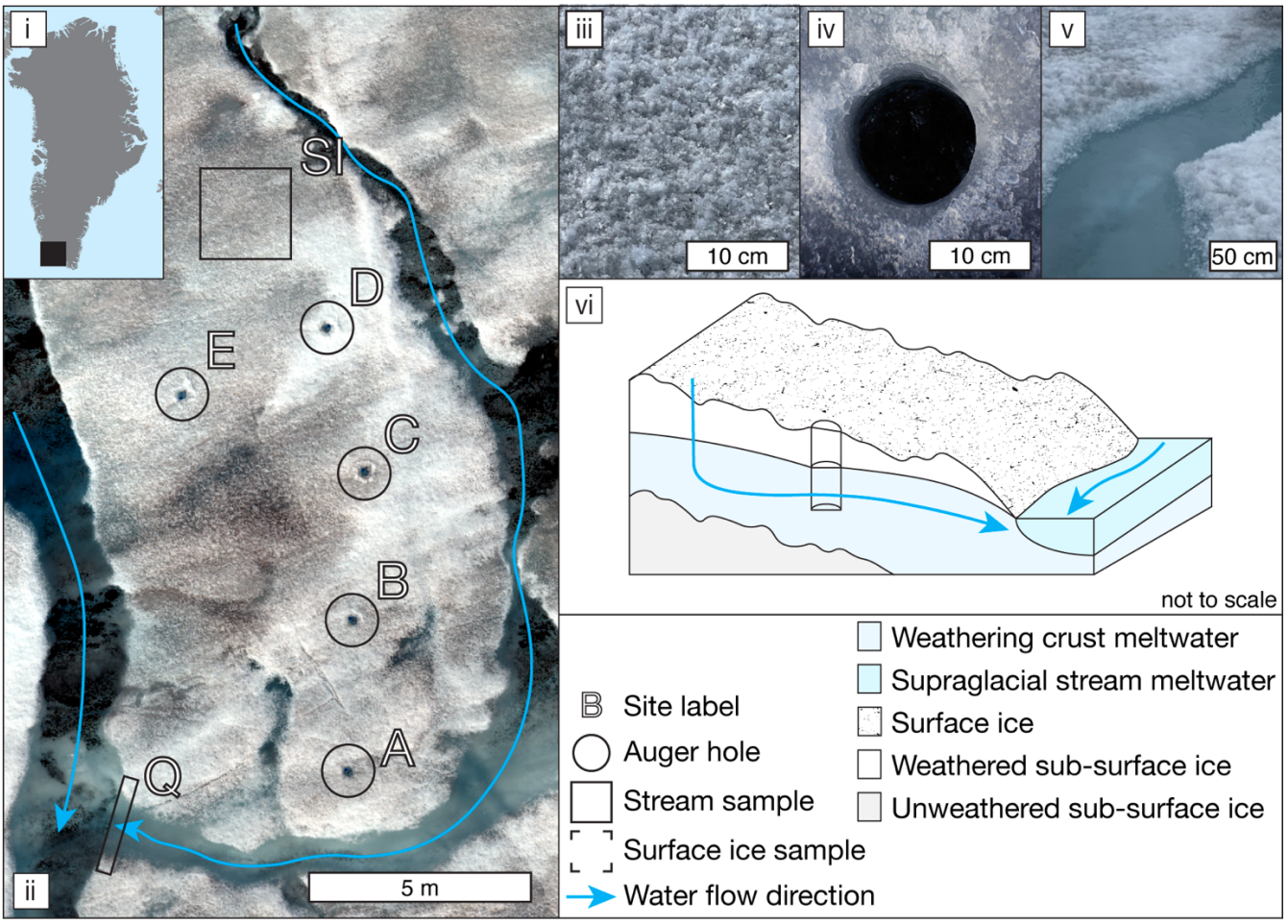

Figure 1: (i) Map of Greenland indicating the approximate location of the study site; (ii) UAV ortho-image of the study catchment, indicating water flow direction and labelled sampling locations; (iii) close-up of typical surface ice, (iv) close-up of typical weathering crust auger hole; (v) close-up of the stream sampling location; and (vi) schematic illustrating meltwater flow paths through sampling area, including an exemplar auger hole.

2.2 Surface ice particulate water extractable organic matter (SIP-WEOM)

Surface ice particulate matter samples were freeze-dried (ScanVac CoolSafe, -110°C) and cryo-milled using stainless-steel sample holders (Retsch MM400). Sample holders were cleaned with Milli-Q and the first aliquot of milled sample was discarded. For each sample, 100 mg of milled material was weighed into acid-cleaned and combusted 4 mL glass vials, in

triplicate, and 1 mL of Milli-Q was added to each vial. Vials were shaken at 500 rpm for 1 hour and then centrifuged at 3200 rpm for 10 minutes. To yield enough volume for solid-phase extraction, the supernatants containing surface ice particulate WEOM (SIP-WEOM) were diluted in 50 mL Milli-Q water and filtered using an acid-washed and combusted glass syringe and pre-rinsed hydrophilic PTFE syringe filters (Acrodisc One, 0.2 μm, Pall). An aliquot for DOC concentration measurements was collected from each extract before combining the triplicates for solid phase extraction (Section 2.4).

2.3 Dissolved organic carbon, total carbon and total nitrogen measurements

DOC concentrations in liquid samples were determined using a Shimadzu TOC-L_{CSH} analyser. Up to five replicate injections were made for each sample until the coefficient of variation (CV) for three of the replicate injections was ≤ 2 %. Measurements were quantified using a potassium hydrogen phthalate (Sigma-Aldrich) calibration curve. The instrument quantification limit (27 μg L^{-1}) was calculated from linear calibrations following the root mean square error method described by Corley (2003). Analytical precision calculated based on the standard error from seven repeat measurements of a 100 μg L^{-1} standard was 1.6 %. Total carbon and total nitrogen content of surface ice particulate matter samples was determined using an Elemental analyser (Euro EA). The limit of quantification was 0.15 %, with a relative standard deviation of <5 %. Total carbon and total nitrogen are reported in weight percent (wt. %).

2.4 Solid phase extraction

All DOM and WEOM samples were solid phase extracted at GFZ Potsdam, Germany, following Dittmar et al. (2008), to remove inorganic interferences and concentrate the organic matter prior to FT-ICR MS analysis. DOM samples were extracted on 6 mL, 1 g, Bond Elut PPL cartridges. WEOM samples were extracted on 3 mL, 100 mg, Bond Elut PPL cartridges. Samples were eluted with 6 mL of methanol into acid-soaked and combusted 10 mL amber glass vials. Eluates were dried under nitrogen flow and stored at -20 °C until analysis.

2.5 21 tesla Fourier transform ion cyclotron resonance mass spectrometry

Dried eluates were reconstituted in methanol prior to analysis, adjusting the volume to achieve a target concentration of 50 mg C L^{-1}. DOM composition was analysed using a custom-built 21 tesla FT-ICR MS at the National High Magnetic Field Laboratory in Tallahassee, Florida (Hendrickson et al., 2015; Smith et al., 2018). Electrospray ionization was used to directly inject negative ions into the FT-ICR MS at a flow rate of 0.5 μL min^{-1} (additional acquisition details in Supplementary Information). One hundred transients were co-added for each sample and signals less than the root mean square baseline plus 6σ were not considered. Mass spectra were calibrated with 10-15 homologous series that span the entire molecular weight distribution based on the "walking" calibration method (Savory et al., 2011) using Predator Analysis software (Blakney et al., 2011), and singly charged ions between 120 and 1,150 Da were assigned molecular formulae within the bounds of $C_{1\text{-}100}H_{4\text{-}200}O_{1\text{-}30}N_{0\text{-}4}S_{0\text{-}2}$ and ± 0.5 ppm error (Table S1). Molecular formulae were classified by heteroatomic content as containing carbon, hydrogen and oxygen only (CHO), or with nitrogen (CHON), sulfur (CHOS), or both N and S (CHONS). Neutral

elemental ratios of H/C and O/C were calculated, classifying constituents with H/C ≥1.5 as biolabile per D'Andrilli et al (2015). The modified aromaticity index (AI_{mod}) was calculated as in Koch and Dittmar (2006, 2016), classifying formulae as aromatic when $AI_{mod} > 0.5$. The nominal oxidation state of carbon (NOSC) was calculated as in Riedel et al (2012), with a negative NOSC corresponding to more reduced formulae and a positive NOSC corresponding to more oxidized ones. Elemental compositions were classified into eight groups: condensed aromatics ($AI_{mod} \geq 0.67$), polyphenols ($0.67 > AI_{mod} > 0.50$), peptide-like formulae (H/C ≥ 1.5, O/C ≤ 0.9, N > 0), sugar-like formulae (H/C ≥ 1.5, O/C > 0.9), and highly unsaturated and phenolic formulae (HUP; $AI_{mod} \leq 0.50$, H/C < 1.5) and aliphatics (H/C ≥ 1.5, O/C ≤ 0.9, N = 0), which were both separated into high O/C (O/C > 0.5) and low O/C (O/C < 0.5) (Osterholz et al., 2016; Spencer et al., 2014). The relative abundance (RA) of each assigned formula in a sample was obtained by dividing the signal magnitude of each individual *m/z* peak by the sum of all assigned signals in the sample. Peaks with RA > 0.1% in the procedural field blank were removed from the dataset as they were assumed to be potential contaminants, and data were renormalized to the total sum of assigned signals. RA weighted metrics were calculated for the mass, $AI_{mod,}$ NOSC, H/C and O/C.

2.6 Statistics

All statistical analyses were performed in R (R Team, 2014). Pairwise comparisons were performed between samples grouped as SIP-WEOM, surface ice, weathering crust meltwater, and supraglacial stream water. The Shapiro-Wilk test was used to assess normality, and Bartlett's test was used to assess homogeneity of variance for all variables. For normally distributed variables, if variance was equal, a one-way ANOVA assuming equal variance was used, followed by pairwise comparison using a t-test if the ANOVA was significant, and p-values were adjusted using Bonferroni correction. If variance was unequal, a one-way ANOVA assuming unequal variance was used, followed by pairwise comparison using a t-test assuming unequal variance if the ANOVA was significant, and p-values were adjusted using Šidák correction. For variables that were non-normally distributed, pairwise comparisons were performed using the non-parametric Wilcoxon rank sum test. Variables were unit variance scaled prior to Principal Component (PC) analysis using the R package 'vegan' (Oksanen et al., 2011).

3 Results

3.1 Near-surface hydrology of the study site

Our hydrological modelling approach reveals that meltwater from auger hole D, where weathering crust meltwater samples were collected, transits from the sampling point within the weathering crust in a south-easterly direction to the main supraglacial stream over a period of nine days (see Fig. 2) assuming the prevailing weather crust state during the study period remains constant.

3.2 Bulk dissolved organic carbon, total carbon, and total nitrogen concentrations

Surface ice DOC concentrations were similar (0.90 - 1.01 mg C L^{-1}) in the four samples collected within the micro-catchment and were significantly higher than the DOC concentrations in weathering crust meltwater and supraglacial stream water (Table 1). The surface ice particulate matter contained between 3.00 – 3.35 wt. % total carbon, and between 0.25 – 0.28 wt. % total nitrogen. The DOC concentrations in SIP-WEOM extracts ranged from 277 – 483 mg C L^{-1}, with a mean CV of 2.4% between triplicate extractions. This corresponds to 7.4 – 12.1 % of total carbon in the freeze-dried and cryo-milled sample extracted as DOC.

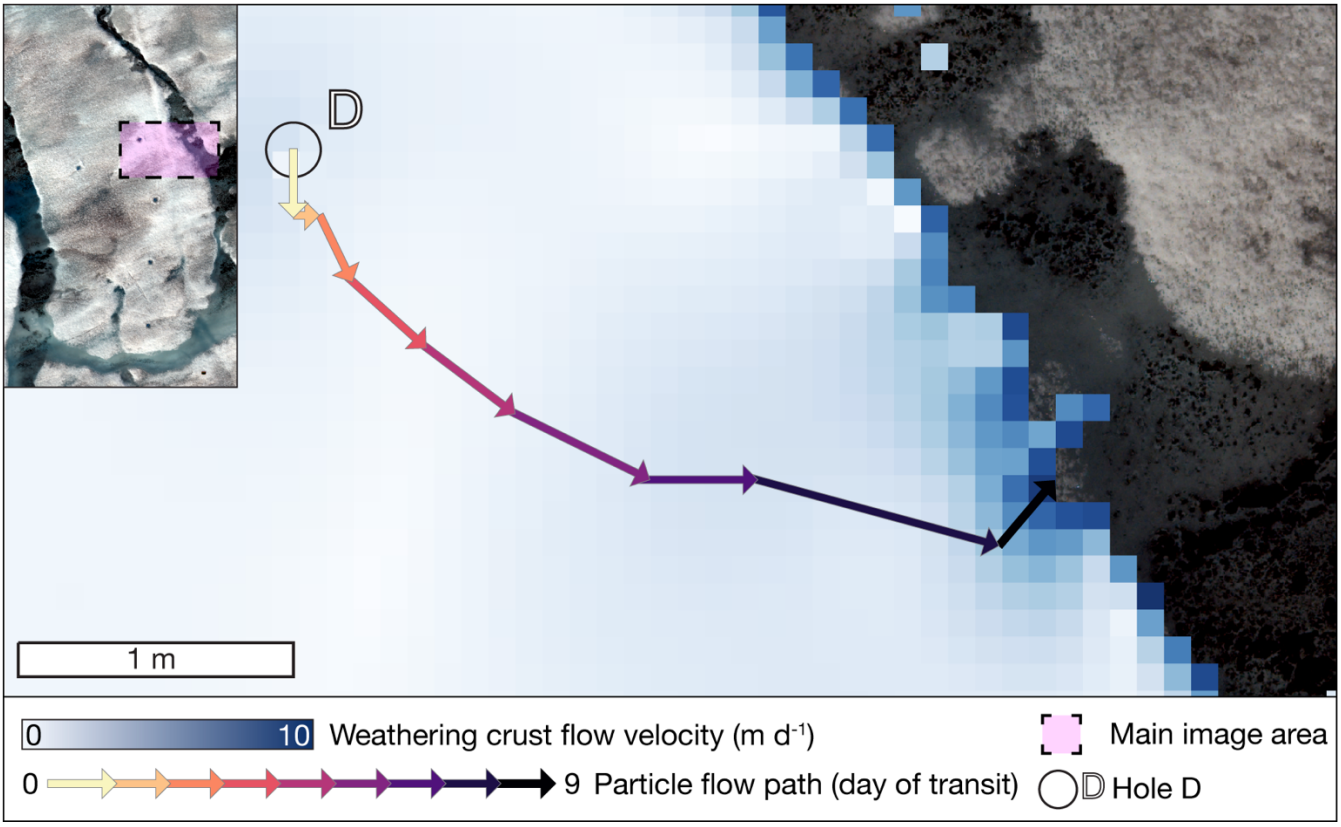

Figure 2: Results of the flow direction and magnitude model, with pixel colour indicating weathering crust water flow velocity. Arrows indicate the modelled particle flow path through the weathering crust from Hole D to the supraglacial stream.

3.3 Molecular level composition of supraglacial DOM and WEOM

A total of 24,578 unique molecular formulae were assigned across the dataset, with between 6,385 and 9,667 formulae assigned in individual samples (Table 1) after blank correction, and 2,885 formulae shared across all samples in the dataset (Figure 3A). In the SIP-WEOM samples, on average 63% (3,653 – 6,053 formulae) of the assigned formulae were also assigned in the

corresponding surface ice DOM. The H/C ratio in surface ice DOM was significantly lower than in the other sample groups (Table 1), corresponding to a significantly lower prevalence of aliphatic and peptide-like formulae (12.8 ± 3.7 %RA) in surface ice DOM than in the rest of the dataset (32.8 – 68.3 %RA). The %RA of heteroatom classes differed significantly between sample types (Table 1). SIP-WEOM was composed of approximately equal portions of CHO (35.9 – 58.0 %RA) and CHOS (33.3 – 55.2 %RA), with relatively minor contributions of CHON (4.9 – 10.6 %RA) and CHONS (0.25 – 0.47 %RA) formulae. Surface ice DOM was predominantly composed of CHO (91.2 – 96.5 %RA), with minor contributions of CHON (3.5 – 6.9 %RA) and CHOS (0 – 1.9 %RA) formulae. The prevalence of CHON in weathering crust meltwater and supraglacial stream DOM was similar (13.9 – 15.5 and 14.9 – 16.7 %RA, respectively), but there was a significant difference in the contribution of CHO (63.3 – 70.5 and 73.6 – 83.8 %RA, respectively) and CHOS (14.5 – 22.1 and 0.6 – 11.5 %RA, respectively). No CHONS formulae were assigned in surface ice, weathering crust meltwater, or supraglacial stream DOM samples.

Aliphatic and HUP formulae made up the majority of DOM in weathering crust and supraglacial stream DOM and SIP-WEOM (Table 1). Aliphatic formulae accounted for approximately half of the SIP-WEOM (46.4 – 62.1 %RA), just under half of weathering crust meltwater DOM (40.8 – 47.4 %RA) and roughly a third of DOM in supraglacial stream samples (28.4 – 38.3 %RA). Surface ice DOM was comprised predominantly of HUP (59.0 – 68.5 %RA) and aromatic (21.8 – 27.5 %RA) formulae. Aromaticity was low, yet variable across the sample groups, with surface ice DOM having significantly higher aromaticity (AI_{mod} 0.305 – 0.340) than SIP-WEOM, weathering crust meltwater DOM and supraglacial stream DOM (AI_{mod} 0.123 – 0.172).

The number of aromatic formulae assigned decreased from surface ice DOM (765 – 957), to weathering crust meltwater DOM (491 – 547), to supraglacial stream water DOM (271 – 420) and SIP-WEOM (153 – 440). The number of biolabile (aliphatic + peptide-like) formulae was highest in SIP-WEOM (2,984 – 3,719) and weathering crust meltwater DOM (3,124 – 3,341), and lowest in surface ice DOM (1,584 – 2,640). The number of biolabile formulae assigned in supraglacial stream DOM (2,498 – 2,890) was similar to that in weathering crust meltwater DOM. The %RA of peptide-like formulae was significantly lower in surface ice (1.3 – 2.8 %RA) than in other sample groups (Table 1).

Table 1: DOC concentrations and DOM composition for each sample group, expressed as mean (standard deviation). %RA = precent relative abundance; # = number of formulae; and wa = RA weighted average.

	SIP-WEOM	Surface ice	Weathering crust	Stream
DOC (mg L^{-1})	386 (85) ^{A}	0.94 (0.05) ^{B}	0.18 (0.04) ^{C}	0.14 (0.01) ^{C}
Formulae (#)	8,403 (864) ^{A}	7,570 (965) ^{A}	9,008 (587) ^{A}	8,343 (1022) ^{A}
$Mass^{wa}$ (Da)	407 (10) ^{A}	450 (10) ^{BC}	429 (9) ^{AB}	452 (12) ^{C}
AI_{mod}^{wa}	0.149 (0.022) ^{A}	0.326 (0.016) ^{B}	0.158 (0.003) ^{A}	0.162 (0.006) ^{A}
$NOSC^{wa}$	-0.652 (0.120) ^{AB}	0.112 (0.061) ^{C}	-0.569 (0.045) ^{A}	-0.470 (0.043) ^{B}
H/C^{wa}	1.471 (0.056) ^{AB}	1.072 (0.033) ^{C}	1.438 (0.013) ^{A}	1.405 (0.019) ^{B}
O/C^{wa}	0.369 (0.039) ^{A}	0.582 (0.019) ^{B}	0.406 (0.018) ^{AC}	0.445 (0.014) ^{C}
CHO (%RA)	47.2 (9.1) ^{A}	94.1 (2.5) ^{B}	68.2 (3.3) ^{C}	81.4 (4.4) ^{D}
CHON (%RA)	8.1 (2.4) ^{A}	5.2 (1.7) ^{A}	14.6 (0.7) ^{B}	15.6 (0.8) ^{B}
CHOS (%RA)	44.3 (9.0) ^{A}	0.7 (0.8) ^{B}	17.2 (3.5) ^{C}	3.0 (4.8) ^{B}
CHONS (%RA)	0.4 (0.1) ^{A}	0.0 (0.0) ^{B}	0.0 (0.0) ^{B}	0.0 (0.0) ^{B}
Aliphatic High O/C (%RA)	5.5 (1.5) ^{AB}	4.3 (1.0) ^{B}	6.9 (0.8) ^{AC}	8.6 (0.6) ^{C}
Aliphatic Low O/C (%RA)	51.0 (6.8) ^{A}	6.6 (2.1) ^{B}	36.8 (3.1) ^{C}	25.1 (3.8) ^{D}
HUP High O/C (%RA)	20.6 (8.2) ^{A}	49.7 (7.3) ^{B}	20.6 (2.6) ^{A}	25.2 (2.9) ^{A}
HUP Low O/C (%RA)	14.8 (1.9) ^{AB}	12.5 (2.8) ^{B}	25.5 (1.1) ^{A}	34.1 (2.1) ^{A}
Peptide-like (%RA)	5.1 (1.9) ^{A}	1.9 (0.7) ^{B}	6.5 (0.6) ^{A}	4.8 (0.6) ^{A}
Condensed aromatic (%RA)	0.4 (0.2) ^{AC}	7.8 (0.9) ^{B}	0.7 (0.1) ^{C}	0.3 (0.1) ^{A}
Polyphenolic (%RA)	2.4 (1.7) ^{AB}	17.1 (2.3) ^{D}	2.7 (0.2) ^{A}	2.0 (0.2) ^{B}
Sugar (%RA)	0.17 (0.10) ^{A}	0.03 (0.02) ^{A}	0.03 (0.02) ^{A}	0.04 (0.02) ^{A}
Aromatic (%RA)	2.8 (1.9) ^{AB}	24.9 (2.8) ^{C}	3.5 (0.3) ^{A}	2.2 (0.2) ^{B}
Aliphatic + peptide-like (%RA)	61.6 (8.1) ^{A}	12.8 (3.7) ^{B}	50.3 (2.4) ^{C}	38.5 (3.9) ^{D}
Aromatic (#)	286 (134) ^{A}	862 (80) ^{B}	523 (24) ^{C}	362 (70) ^{AC}
Aliphatic + peptide-like (#)	3,395 (320) ^{A}	2,088 (464) ^{B}	3,228 (119) ^{AC}	2,698 (148) ^{C}

Data were plotted in van Krevelen space to visualize the molecular composition of the core supraglacial DOM signature (see Fig. 3A) and the different sample groups (see Fig. 3B-E). The core supraglacial DOM signature is made up of predominantly HUP and aliphatic formulae with the heteroatomic formula CHO or CHON, and accounts for on average 41.8 %RA of SIP-WEOM, 67.9 %RA of surface ice DOM, 58.6 %RA of weathering crust meltwater DOM and 72.2 %RA of supraglacial stream DOM. To visualize the difference between SIP-WEOM and DOM in surface ice, weathering crust meltwater and supraglacial stream meltwater, formulae that were assigned in all samples in a sample group but were not present in the core supraglacial DOM signature were plotted in Fig. 3B-E. The SIP-WEOM signature contained 1,509 formulae (Fig. 3B) predominantly occupying the aliphatic and HUP space in the van Krevelen diagram, and accounting for 37.4 – 55.6 %RA of SIP-WEOM. The surface ice DOM signature contained 2,577 formulae accounting for 23.9 – 29.6 %RA, with most formulae falling in the HUP region of the van Krevelen diagram (Fig. 3C) and a clear contribution of polyphenolic and condensed aromatic formulae. The weathering crust meltwater DOM signature contained the largest number of formulae (3,995), accounting for 33.8 – 39.2 %RA and falling mostly in the aliphatic and HUP space, with ~52% of formulae containing nitrogen. The supraglacial stream DOM signature was most similar to the weathering crust meltwater signature, but with fewer formulae (3,099) in all regions of the van Krevelen diagram and formulae accounting for only 16.5 – 19.4 %RA of stream DOM. To further examine the differences between weathering crust and supraglacial stream meltwater DOM, formulae present in all weathering crust meltwater samples but not in any of the supraglacial stream samples are plotted in Fig. 3F, where approximately 60% of the formulae fall in the aliphatic region and contain sulphur or nitrogen, but only account for 0.8 – 1.2 %RA of weathering crust DOM. Across the entire dataset, only 24 formulae were present in all supraglacial stream samples but not in any weathering crust meltwater samples.

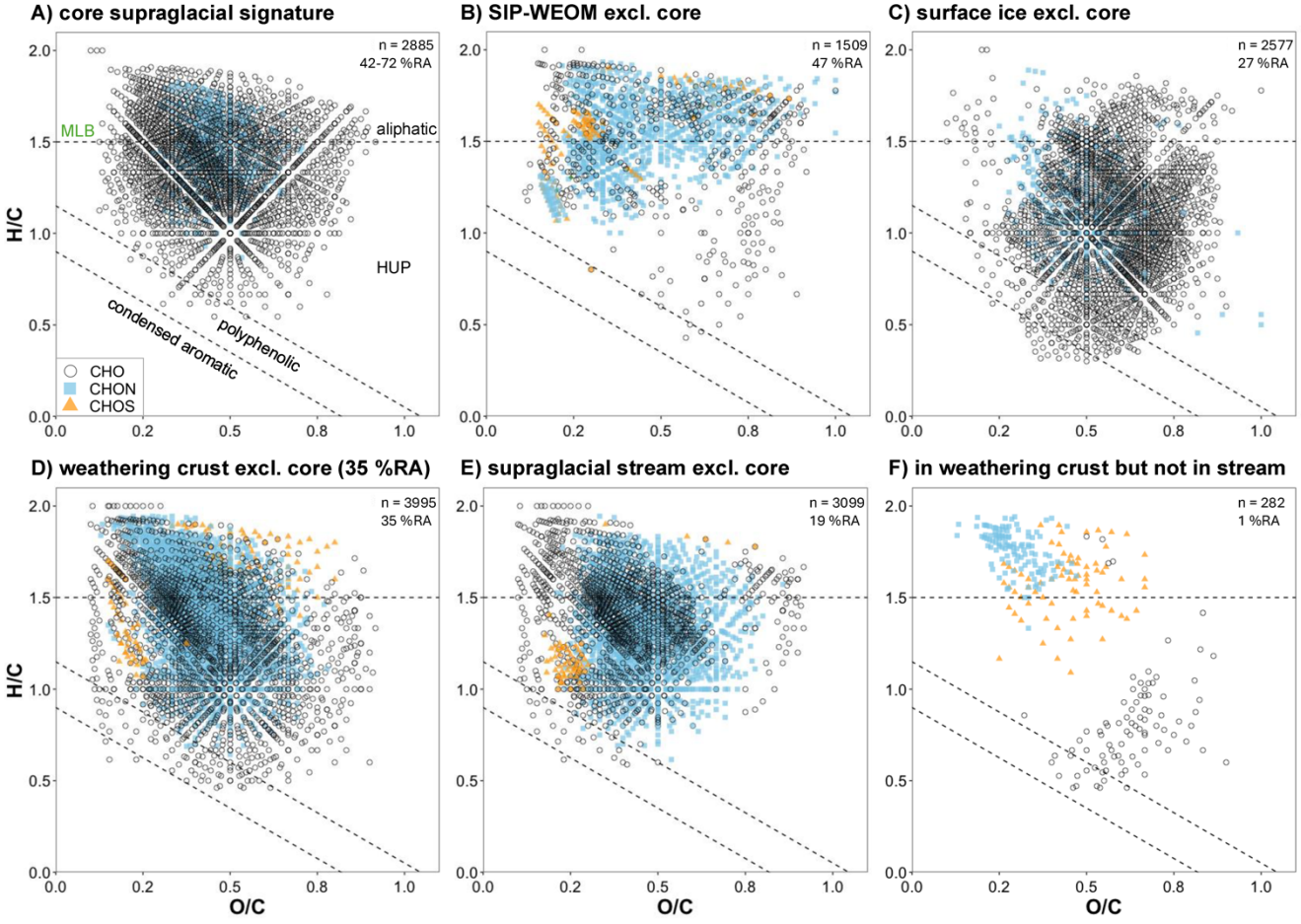

Figure 3: van Krevelen diagrams showing: (A) the core supraglacial signature, showing formulae that were assigned in all samples in the dataset; (B) formulae that were assigned in all SIP-WEOM samples, excluding those present in the core supraglacial signature; (C) formulae that were assigned in all surface ice DOM samples, excluding those present in the core supraglacial signature; (D) formulae that were assigned in all weathering crust meltwater DOM samples, excluding those present in the core supraglacial signature; (E) formulae that were assigned in all supraglacial samples, excluding those present in the core supraglacial signature; and (F) formulae that were assigned in all weathering crust DOM samples but not in any supraglacial stream DOM samples. Data points are coloured according to their assigned heteroatom class with CHO formulae in black open circles, CHON in light blue squares, and CHOS in orange triangles. In the top right of each panel, the total number of formulae displayed in the diagram and the average %RA accounted for by those formulae is denoted. Dashed lines indicate the regions corresponding to condensed aromatic, polyphenolic, highly unsaturated and phenolic (HUP) and aliphatic formulae. Note that the dashed line separating the HUP and aliphatic regions corresponds to the Molecular Lability Boundary (MLB) as proposed by D'Andrilli et al. (2015), where DOM constituents with H/C ≥ 1.5 are considered labile.

3.3 Compositional differences between hydrologically connected DOM pools

To examine the DOM parameters that distinguish the different sample groups, we conducted a principal component (PC) analysis on all samples (Fig. 4, Table S2). PC1 explained 63% of variance in the data and correlated positively with NOSC,

AI_{mod}, the %RA of high O/C HUP, condensed aromatic and polyphenolic formulae, %RA of CHO, and mean RA weighed mass. PC1 correlated negatively with number of formulae, the %RA of peptide-like, low and high O/C aliphatic and low O/C HUP formulae, and %RA of CHON and CHOS. Surface ice DOM separated from the other sample groups along PC1, reflecting its significantly higher aromaticity and lower %RA of biolabile peptide-like and aliphatic formulae (Table 1). PC2 explained a further 26% of variance in the data, correlating positively with %RA of low O/C HUP and high O/C aliphatic formulae, %RA of CHO and CHON, and mean RA weighted mass. Finally, PC2 correlated negatively with %RA of low O/C aliphatic formulae and %RA CHOS. SIP-WEOM, weathering crust meltwater and supraglacial stream DOM separate along PC2, with the former containing a significantly higher %RA of CHOS formulae and %RA of low O/C aliphatic formulae (Table 1). Weathering crust meltwater and supraglacial stream samples formed two separate clusters, driven by significant differences in prevalence of low O/C aliphatic formulae, and sulphur-containing formulae. The PC analysis showed clear a clustering of sample groups based on DOM parameters.

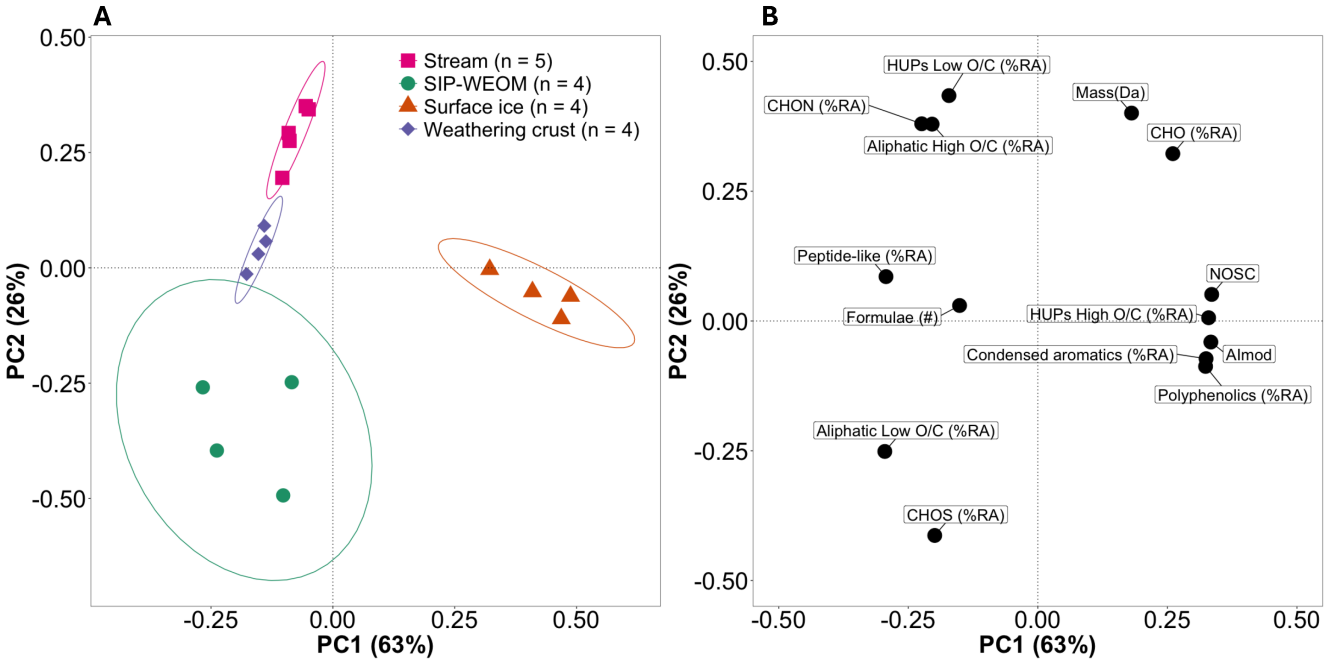

Figure 4: (A) Principal component (PC) analysis scores plot of DOM composition in SIP-WEOM (green circles), surface ice (orange triangles), weathering crust meltwater (purple diamonds) and supraglacial stream water (pink squares) samples, with ellipses representing 90% confidence intervals; and (B) loadings plot of the variables included in the PC analysis. %RA = percent relative abundance; # = number of formulae; NOSC = nominal oxidation state of carbon; AI_{mod} = modified aromaticity index; HUP = highly unsaturated and phenolic formulae; CHO, CHON and CHOS refer to heteroatomic composition with carbon (C), nitrogen (N), oxygen (O) and sulphur (S).

4 Discussion

4.1 Hydrological connectivity of supraglacial meltwater habitats

In the studied micro-catchment, modelled lateral interstitial flow velocity through the weathering crust was in the order of decimetres per day, corresponding with estimates from Stevens et al. (2018), Irvine-Fynn et al. (2021) and Yang et al. (2018). The particle track from auger hole D (Fig. 2) confirmed the assumed hydrological connections between sampling locations. We assume that water sampled from the weathering crust auger holes was comprised of a mixture of recent melt, originating near the hole, and meltwater already transiting within the weathering crust. We also assume the addition of further meltwater, percolating from the unsaturated zone of the weathering crust, along the transit pathway from auger hole D to the supraglacial stream (Fig. 1v). The presence of a core supraglacial DOM signature (Fig. 3A) supports the assumption that the surface ice, weathering crust meltwater and supraglacial stream habitats, and hence DOM pools, may be hydrologically connected. The indicative value of nine days for meltwater flow through the weathering crust to the supraglacial stream allows the possibility of modification of the DOM pool via microbial reworking and/or photochemical degradation (Antony et al., 2017, 2018; Holt et al., 2021; Riedel et al., 2016).

4.2 DOM cycling in the supraglacial weathering crust

Characterization of weathering crust meltwater, supraglacial stream and surface ice DOM revealed compositional differences between the three samples groups, with samples of the same type grouping together in the PC analysis score plot (Fig. 4A). Firstly, there is a significant decrease in the %RA of aromatic formulae from surface ice to weathering crust meltwater to supraglacial stream water, likely due to photodegradation (Maurischat et al., 2023; Spencer et al., 2009; Stubbins et al., 2010). The small but significant different in %RA of aromatic formulae between weathering crust and supraglacial stream meltwater DOM suggest that photodegradation not only takes place on the ice surface, but also in the weathering crust photic zone. This is probable given the penetration of solar radiation to depths of 1–2 m within the ice surface (Irvine-Fynn and Edwards, 2014) and the estimated nine days of water transit time between the auger hole where the weathering crust meltwater was sampled and the supraglacial stream. Furthermore, the significantly higher RA weighted average mass and significantly lower %RA of aliphatic + peptide-like formulae in supraglacial stream DOM compared to weathering crust meltwater DOM point at microbial respiration of labile DOM as meltwater transits through the weathering crust before entering the supraglacial stream by the active (Christner, 2018) and diverse (Rassner et al., 2024) weathering crust bacterial community. Finally, only twelve formulae, accounting for 0.02 – 0.05 %RA of supraglacial stream DOM, were assigned in supraglacial stream samples but not in any other sample in this study. Hence, we postulate that the differences between weathering crust meltwater and supraglacial stream DOM are not due to upstream snowmelt inputs into the supraglacial stream but are rather the result of photodegradation and microbial reworking of DOM during meltwater transit through the weathering crust and into the supraglacial stream.

Given the hydrological connectivity of surface ice with weathering crust meltwaters, a higher degree of convergence between surface ice and weathering crust meltwater DOM may be expected. The higher concentration of DOC in surface ice relative to weathering crust meltwater may be due to dilution of surface DOC in the weathering crust by meltwater produced in the subsurface and percolating from the unsaturated zone of the weathering crust. However, the sampled weathering crust meltwater contains a mixture of recent melt and meltwater already transiting within the weathering crust, which has already been exposed to photodegradation and/or microbial reworking within the weathering crust photic zone, contributing to the divergence between surface ice and weathering crust DOM. In addition, partial and/or temporary retention of DOM via association with surface ice extracellular polymeric substances (EPS), as suggested by Holland et al. (2019), may further contribute to the divergence between surface ice and weathering crust DOM. EPS have been shown to play a role in the formation of granules in supraglacial cyanobacteria communities (Langford et al., 2010; Stibal et al., 2012; Yallop et al., 2012) and Perini et al. (2023) observed glacier ice algae embedded in EPS during co-cultivation with the surface ice fungi *Articulospora* sp. To date, the chemical composition and role of EPS in surface ice microbial communities, and the degree to which DOM sourced from atmospheric deposition, microbial activity or cell lysis may be retained on the ice surface, remain unknown.

4.3 Surface ice particulate matter as a source of supraglacial DOM

Surface ice DOM is a complex mixture sourced from microbes (including EPS), atmospheric deposition and melt-out of material contained within the ablating glacier surface. The presence of an active microbial community (Anesio et al., 2017) and the high solar irradiance received by the ice sheet surface during the boreal summer mean that microbial reworking and photodegradation, respectively, of DOM is likely to impact the composition of surface ice DOM. Retention of DOM on the ice surface via association with EPS would increase the duration of its exposure to photodegradation and/or microbial reworking on the ice surface. Hence, analysis of surface ice DOM does not provide clear insights into the role of surface ice particulate matter as a supraglacial source of DOM. To gain insights into the DOM that may be sourced from surface ice particulate matter, we isolated and characterized SIP-WEOM. The SIP-WEOM extract DOC accounted for on average 9.6% of surface ice particulate matter total carbon, likely with a significant contribution of material yielded from the lysis of cells as the result of freeze-drying and cryo-milling of the particulate matter prior to extraction. The presence of DOM from microbial sources (Kellerman et al., 2018; Spencer et al., 2015) is reflected in SIP-WEOM having a significantly higher contribution of aliphatic and peptide-like formulae that any other sample group in this study. This provides direct evidence of surface ice particulate matter, which include microbes, as a supraglacial source of biolabile DOM.

Surface ice DOM and SIP-WEOM were found to cluster into two different groups (Fig. 4A) based on their DOM parameters, likely due to surface ice DOM having multiple sources, microbial reworking of surface ice DOM and/or photodegradation. Surface ice DOM had a significantly higher aromaticity, with a quarter of surface ice DOM comprised of aromatic formulae.

Of this aromatic DOM, 5.7 – 8.8 %RA is accounted for by the molecular formula $C_{12}H_8O_7$. A potential compound that could give rise to the presence of this formula is the aglycone derivative of the algal pigment purpurogallin carboxylic acid-6-O-β-D-glucopyranoside, produced by the algae *Ancylonema alaskanum* and *Ancylonema nordenskiöldii*, which dominate the surface ice microbial community (Procházková et al., 2021). Fungal parasitic infections, which were found to impact approximately 25% of algal cells collected from a High Arctic, can result in the loss of pigment from the algal cells (Fiołka et al., 2021). The sugar moiety of the purpurogallin pigment can be utilized as an energy source, for example, by the surface ice fungal species *P. anthracinoglaciei* (Perini et al., 2023), converting the pigment into its aglycone derivative and likely contributing to the higher %RA of aromatic formulae in surface ice DOM.

Furthermore, 6.4 ± 0.8 %RA in surface ice DOM is comprised of condensed aromatic ring structures with O/C > 0.4, which have been linked with microbially mediated oxidation of black carbon (Antony et al., 2014; Dittmar and Koch, 2006). This suggests that a portion of surface ice DOM may be sourced from microbial oxidation of black carbon to form water-soluble species (Hockaday et al., 2006). As the contribution of condensed aromatic formulae to weathering crust and supraglacial stream meltwater DOM is near zero, it appears that such water-soluble black carbon species are not exported from the ice surface to downstream ecosystems. Yet, radiocarbon-depleted DOM sourced from black carbon may still be exported in supraglacial runoff, given that photodegradation of aromatic formulae can produce aliphatic and peptide-like formulae (Holt et al., 2021), and that weathering crust and supraglacial stream meltwater DOM contain a higher number and %RA of aliphatic and peptide-like formulae than surface ice. Radiocarbon analysis of surface ice particulate matter and supraglacial meltwater habitats is needed to assess the role of the supraglacial drainage system in exporting radiocarbon-depleted DOM to downstream ecosystems.

5 Conclusions

Over the last decade, numerous studies have highlighted the role of the supraglacial weathering crust in the storage and release of meltwater (Müller and Keeler, 1969) and microbes (Irvine-Fynn, 2012; Irvine-Fynn and Edwards, 2014). Nevertheless, to date, biogeochemical cycling within the weathering crust has not been assessed, limiting our understanding of how the export of supraglacial DOM to downstream ecosystems may change in a warming climate. Here, we reveal that the weathering crust plays a role in the cycling of DOM during supraglacial transit of meltwater. We characterise DOM along a meltwater flow path in a hydrologically connected micro-catchment on the Southern Greenland Ice Sheet, revealing compositional differences between surface ice, weathering crust and supraglacial stream meltwater. Decreases in the %RA of aromatic formulae from surface ice to weathering crust to supraglacial stream meltwater point towards photodegradation of DOM on the ice surface and during transport through the weathering crust photic zone. The lower %RA of aliphatic and peptide-like formulae and RA weighted average mass of supraglacial stream relative to weathering crust meltwater DOM are likely a result of respiration of DOM by active and diverse (Christner, 2018; Rassner et al., 2024) bacterial communities. Furthermore, we characterize

WEOM isolated from surface ice particulate matter, presenting the first direct evidence of surface ice particulate matter as a potential supraglacial source of biolabile DOM. As the spatial extent of the weathering crust photic zone and the frequency of weathering crust degradation events as a result of rainfall are set to increase as a result of climatic warming, further studies of the role of the weathering crust in biogeochemical cycles are urgently required to enable predictions of future changes in the export of supraglacial DOM to downstream ecosystems.

Data availability

All FT-ICR MS data used in this study can be found in the Open Science Framework Repository via DOI 10.17605/OSF.IO/JRBTH.

Author contributions

Study design, conceptualisation, and sample collection was done by ELD and ITS. Field processing was done by PER. DOC, TC and TN analysis was done by RA. Lab set-up for DOM extractions was done by ELD and PER. Sample preparation was done by ELD. FT-ICR MS data acquisition was done by AMM. Molecular formula assignment and classification was done by AMK. Hydrological data processing was done by ITS. Data analysis and manuscript preparation was done by ELD. All authors contributed to the final manuscript with discussion and revisions.

Competing interests: The authors declare that they have no conflict of interest.

Acknowledgements

This study was financially supported by the European Research Council (ERC) Synergy Grant DEEP PURPLE under the European Union's Horizon 2020 research and innovation programme (grant agreement No 856416), the Aarhus University Research Foundation through a Starting Grant for AMA (AUFF-2018), the Aarhus University Interdisciplinary Centre for Climate Change (iClimate), and the network programme of the Danish Agency for Science and Higher Education (9096-00101B) and the Helmholtz Recruiting Initiative grant (award # I-044-16-01 to LGB). RA acknowledges funding from the Alexander von Humboldt Foundation, and RGMS would like to acknowledge NSF DEB 1145932. A portion of this work was performed in the Ion Cyclotron Resonance User Facility at the National High Magnetic Field Laboratory, which is supported by the National Science Foundation Division of Chemistry and Division of Materials Research through DMR-2128556 and the State of Florida. All 21 T FT-ICR MS files are publicly available via the Open Science Framework through DOI 10.17605/OSF.IO/JRBTH. Predator analysis and PetroOrg© software is publicly available for ICR facility users at https://nationalmaglab.org/user-facilities/icr/icr-software. Finally, the authors would like to thank the entire DEEP PURPLE team, especially those involved in the 2021 field campaign.

References

Anesio, A. M., Lutz, S., Chrismas, N. A. M., and Benning, L. G.: The microbiome of glaciers and ice sheets, Npj Biofilms Microbiomes, 3, 10, https://doi.org/10.1038/s41522-017-0019-0, 2017.

Antony, R., Grannas, A. M., Willoughby, A. S., Sleighter, R. L., Thamban, M., and Hatcher, P. G.: Origin and sources of dissolved organic matter in snow on the east antarctic ice sheet, Environ. Sci. Technol., 48, 6151–6159, https://doi.org/10.1021/ES405246A/SUPPL_FILE/ES405246A_SI_002.XLSX, 2014.

Antony, R., Willoughby, A. S., Grannas, A. M., Catanzano, V., Sleighter, R. L., Thamban, M., Hatcher, P. G., and Nair, S.: Molecular Insights on Dissolved Organic Matter Transformation by Supraglacial Microbial Communities, Environ. Sci. Technol., 51, 4328–4337, https://doi.org/10.1021/ACS.EST.6B05780/SUPPL_FILE/ES6B05780_SI_002.XLS, 2017.

Antony, R., Willoughby, A. S., Grannas, A. M., Catanzano, V., Sleighter, R. L., Thamban, M., and Hatcher, P. G.: Photo-biochemical transformation of dissolved organic matter on the surface of the coastal East Antarctic ice sheet, Biogeochemistry, 141, 229–247, https://doi.org/10.1007/S10533-018-0516-0/FIGURES/3, 2018.

Arnold, N. S., Banwell, A. F., and Willis, I. C.: High-resolution modelling of the seasonal evolution of surface water storage on the Greenland Ice Sheet, The Cryosphere, 8, 1149–1160, https://doi.org/10.5194/tc-8-1149-2014, 2014.

Bardgett, R. D., Richter, A., Bol, R., Garnett, M. H., Bäumler, R., Xu, X., Lopez-Capel, E., Manning, D. A. C., Hobbs, P. J., Hartley, I. R., and Wanek, W.: Heterotrophic microbial communities use ancient carbon following glacial retreat, Biol. Lett., 3, 487–490, https://doi.org/10.1098/RSBL.2007.0242, 2007.

Barker, J. D., Sharp, M. J., and Turner, R. J.: Using synchronous fluorescence spectroscopy and principal components analysis to monitor dissolved organic matter dynamics in a glacier system, Hydrol. Process., 23, 1487–1500, https://doi.org/10.1002/HYP.7274, 2009.

Bhatia, M. P., Das, S. B., Longnecker, K., Charette, M. A., and Kujawinski, E. B.: Molecular characterization of dissolved organic matter associated with the Greenland ice sheet, Geochim. Cosmochim. Acta, 74, 3768–3784, https://doi.org/10.1016/j.gca.2010.03.035, 2010.

Blakney, G. T., Hendrickson, C. L., and Marshall, A. G.: Predator data station: A fast data acquisition system for advanced FT-ICR MS experiments, Int. J. Mass Spectrom., 306, 246–252, https://doi.org/10.1016/j.ijms.2011.03.009, 2011.

Christner, B.: Microbial processes in the weathering crust aquifer of a temperate glacier, Cryosphere, 12, 3653–3669, https://doi.org/10.5194/tc-12-3653-2018, 2018.

Chu, V. W.: Greenland ice sheet hydrology: A review, Prog. Phys. Geogr. Earth Environ., 38, 19–54, https://doi.org/10.1177/0309133313507075, 2014.

Cook, J. M., Hodson, A. J., and Irvine-Fynn, T. D. L.: Supraglacial weathering crust dynamics inferred from cryoconite hole hydrology, Hydrol. Process., 30, 433–446, https://doi.org/10.1002/HYP.10602, 2015.

Corley, J.: Best practices in establishing detection and quantification limits for pesticide residues in foods, in: Handbook of residue analytical methods for agrochemicals, Wiley, 59–74, 2003.

D'Andrilli, J., Cooper, W. T., Foreman, C. M., and Marshall, A. G.: An ultrahigh-resolution mass spectrometry index to estimate natural organic matter lability, Rapid Commun. Mass Spectrom., 29, 2385–2401, https://doi.org/10.1002/RCM.7400, 2015.

Dittmar, T. and Koch, B. P.: Thermogenic organic matter dissolved in the abyssal ocean, Mar. Chem., 102, 208–217, https://doi.org/10.1016/j.marchem.2006.04.003, 2006.

Dittmar, T., Koch, B., Hertkorn, N., and Kattner, G.: A simple and efficient method for the solid-phase extraction of dissolved organic matter (SPE-DOM) from seawater, Limnol. Oceanogr. Methods, 6, 230–235, https://doi.org/10.4319/lom.2008.6.230, 2008.

Dou, T. F., Pan, S. F., Bintanja, R., and Xiao, C. D.: More Frequent, Intense, and Extensive Rainfall Events in a Strongly Warming Arctic, Earths Future, 10, e2021EF002378, https://doi.org/10.1029/2021EF002378, 2022.

Fausto, R. S., Van As, D., Mankoff, K. D., Vandecrux, B., Citterio, M., Ahlstrøm, A. P., Andersen, S. B., Colgan, W., Karlsson, N. B., Kjeldsen, K. K., Korsgaard, N. J., Larsen, S. H., Nielsen, S., Pedersen, A., Shields, C. L., Solgaard, A. M., and Box, J. E.: Programme for Monitoring of the Greenland Ice Sheet (PROMICE) automatic weather station data, Earth Syst. Sci. Data, 13, 3819–3845, https://doi.org/10.5194/ESSD-13-3819-2021, 2021.

Fellman, J. B., Hood, E., Raymond, P. A., Stubbins, A., and Spencer, R. G. M.: Spatial Variation in the Origin of Dissolved Organic Carbon in Snow on the Juneau Icefield, Southeast Alaska, Environ. Sci. Technol., 49, 11492–11499, https://doi.org/10.1021/ACS.EST.5B02685/SUPPL_FILE/ES5B02685_SI_001.PDF, 2015.

Fiołka, M. J., Takeuchi, N., Sofińska-Chmiel, W., Wójcik-Mieszawska, S., Irvine-Fynn, T., and Edwards, A.: Morphological and spectroscopic analysis of snow and glacier algae and their parasitic fungi on different glaciers of Svalbard, Sci. Rep. 2021 111, 11, 1–18, https://doi.org/10.1038/s41598-021-01211-8, 2021.

Hendrickson, C. L., Quinn, J. P., Kaiser, N. K., Smith, D. F., Blakney, G. T., Chen, T., Marshall, A. G., Weisbrod, C. R., and Beu, S. C.: 21 Tesla Fourier Transform Ion Cyclotron Resonance Mass

Spectrometer: A National Resource for Ultrahigh Resolution Mass Analysis, J. Am. Soc. Mass Spectrom., 26, 1626–1632, https://doi.org/10.1007/s13361-015-1182-2, 2015.

Hockaday, W. C., Grannas, A. M., Kim, S., and Hatcher, P. G.: Direct molecular evidence for the degradation and mobility of black carbon in soils from ultrahigh-resolution mass spectral analysis of dissolved organic matter from a fire-impacted forest soil, Org. Geochem., 37, 501–510, https://doi.org/10.1016/J.ORGGEOCHEM.2005.11.003, 2006.

Holland, A. T., Williamson, C. J., Sgouridis, F., Tedstone, A. J., McCutcheon, J., Cook, J. M., Poniecka, E., Yallop, M. L., Tranter, M., and Anesio, A. M.: Dissolved organic nutrients dominate melting surface ice of the Dark Zone (Greenland Ice Sheet), Biogeosciences, 16, 3283–3296, https://doi.org/10.5194/bg-16-3283-2019, 2019.

Holt, A. D., Kellerman, A. M., Li, W., Stubbins, A., Wagner, S., McKenna, A., Fellman, J., Hood, E., and Spencer, R. G. M.: Assessing the Role of Photochemistry in Driving the Composition of Dissolved Organic Matter in Glacier Runoff, J. Geophys. Res. Biogeosciences, 126, e2021JG006516, https://doi.org/10.1029/2021JG006516, 2021.

Holt, A. D., Kellerman, A. M., Battin, T. I., McKenna, A. M., Hood, E., Andino, P., Crespo-Pérez, V., Peter, H., Schön, M., De Staercke, V., Styllas, M., Tolosano, M., and Spencer, R. G. M.: A Tropical Cocktail of Organic Matter Sources: Variability in Supraglacial and Glacier Outflow Dissolved Organic Matter Composition and Age Across the Ecuadorian Andes, J. Geophys. Res. Biogeosciences, 128, 1–18, https://doi.org/10.1029/2022JG007188, 2023.

Hood, E., Fellman, J., Spencer, R. G. M., Hernes, P. J., Edwards, R., Damore, D., and Scott, D.: Glaciers as a source of ancient and labile organic matter to the marine environment, Nature, 462, 1044–1047, https://doi.org/10.1038/nature08580, 2009.

Irvine-Fynn, T.: Microbial cell budgets of an Arctic glacier surface quantified using flow cytometry, Env. Microbiol, 14, 2998–3012, https://doi.org/10.1111/j.1462-2920.2012.02876.x, 2012.

Irvine-Fynn, T. D. L. and Edwards, A.: A frozen asset: The potential of flow cytometry in constraining the glacial biome, Cytometry A, 85, 3–7, https://doi.org/10.1002/cyto.a.22411, 2014.

Irvine-Fynn, T. D. L., Edwards, A., Stevens, I. T., Mitchell, A. C., Bunting, P., Box, J. E., Cameron, K. A., Cook, J. M., Naegeli, K., Rassner, S. M. E., Ryan, J. C., Stibal, M., Williamson, C. J., and Hubbard, A.: Storage and export of microbial biomass across the western Greenland Ice Sheet, Nat. Commun. 2021 121, 12, 1–11, https://doi.org/10.1038/s41467-021-24040-9, 2021.

Kellerman, A. M., Guillemette, F., Podgorski, D. C., Aiken, G. R., Butler, K. D., and Spencer, R. G. M.: Unifying Concepts Linking Dissolved Organic Matter Composition to Persistence in Aquatic Ecosystems, Environ. Sci. Technol., 52, 2538–2548, https://doi.org/10.1021/ACS.EST.7B05513/SUPPL_FILE/ES7B05513_SI_001.PDF, 2018.

Kellerman, A. M., Vonk, J., McColaugh, S., Podgorski, D. C., van Winden, E., Hawkings, J. R., Johnston, S. E., Humayun, M., and Spencer, R. G. M.: Molecular Signatures of Glacial Dissolved Organic Matter From Svalbard and Greenland, Glob. Biogeochem. Cycles, 35, e2020GB006709, https://doi.org/10.1029/2020GB006709, 2021.

Koch, B. P. and Dittmar, T.: From mass to structure: an aromaticity index for high-resolution mass data of natural organic matter, Rapid Commun. Mass Spectrom., 20, 926–932, https://doi.org/10.1002/RCM.2386, 2006.

Koch, B. P. and Dittmar, T.: From mass to structure: an aromaticity index for high-resolution mass data of natural organic matter, Rapid Commun. Mass Spectrom., 30, 250–250, https://doi.org/10.1002/RCM.7433, 2016.

Langford, H., Hodson, A., Banwart, S., and Bøggild, C.: The microstructure and biogeochemistry of Arctic cryoconite granules, Ann. Glaciol., 51, 87–94, https://doi.org/10.3189/172756411795932083, 2010.

Lawson, E. C., Bhatia, M. P., Wadham, J. L., and Kujawinski, E. B.: Continuous summer export of nitrogen-rich organic matter from the greenland ice sheet inferred by ultrahigh resolution mass spectrometry, Environ. Sci. Technol., 48, 14248–14257, https://doi.org/10.1021/ES501732H/SUPPL_FILE/ES501732H_SI_001.PDF, 2014a.

Lawson, E. C., Wadham, J. L., Tranter, M., Stibal, M., Lis, G. P., Butler, C. E. H., Laybourn-Parry, J., Nienow, P., Chandler, D., and Dewsbury, P.: Greenland ice sheet exports labile organic carbon to the arctic oceans, Biogeosciences, 11, 4015–4028, https://doi.org/10.5194/bg-11-4015-2014, 2014b.

Li, C., Chen, P., Kang, S., Yan, F., Tripathee, L., Wu, G., Qu, B., Sillanpää, M., Yang, D., Dittmar, T., Stubbins, A., and Raymond, P. A.: Fossil Fuel Combustion Emission From South Asia Influences Precipitation Dissolved Organic Carbon Reaching the Remote Tibetan Plateau: Isotopic and Molecular Evidence, J. Geophys. Res. Atmospheres, 123, 6248–6258, https://doi.org/10.1029/2017JD028181, 2018.

Maurischat, P., Seidel, M., Dittmar, T., and Guggenberger, G.: Complex dissolved organic matter (DOM) on the roof of the world – Tibetan DOM molecular characteristics indicate sources, land use effects, and processing along the fluvial–limnic continuum, Biogeosciences, 20, 3011–3026, https://doi.org/10.5194/bg-20-3011-2023, 2023.

Müller, F. and Keeler, C. M.: Errors in Short-Term Ablation Measurements on Melting Ice Surfaces, J. Glaciol., 8, 91–105, https://doi.org/10.3189/S0022143000020785, 1969.

Musilova, M., Tranter, M., Wadham, J., Telling, J., Tedstone, A., and Anesio, A. M.: Microbially driven export of labile organic carbon from the Greenland ice sheet, Nat. Geosci., 10, 360–365, https://doi.org/10.1038/ngeo2920, 2017.

Niwano, M., Box, J. E., Wehrlé, A., Vandecrux, B., Colgan, W. T., and Cappelen, J.: Rainfall on the Greenland Ice Sheet: Present-Day Climatology From a High-Resolution Non-Hydrostatic Polar Regional Climate Model, Geophys. Res. Lett., 48, e2021GL092942, https://doi.org/10.1029/2021GL092942, 2021.

Oksanen, A. J., Blanchet, F. G., Friendly, M., Kindt, R., Legendre, P., Mcglinn, D., Minchin, P. R., Hara, R. B. O., Simpson, G. L., Solymos, P., Stevens, M. H. H., and Szoecs, E.: Vegan: Community ecology package, 2011.

Osterholz, H., Kirchman, D. L., Niggemann, J., and Dittmar, T.: Environmental drivers of dissolved organic matter molecular composition in the Delaware estuary, Front. Earth Sci., 4, 95, https://doi.org/10.3389/FEART.2016.00095/BIBTEX, 2016.

Perini, L., Gostinčar, C., Likar, M., Frisvad, J. C., Kostanjšek, R., Nicholes, M., Williamson, C., Anesio, A. M., Zalar, P., and Gunde-Cimerman, N.: Interactions of Fungi and Algae from the Greenland Ice Sheet, Microb. Ecol., 86, 282–296, https://doi.org/10.1007/s00248-022-02033-5, 2023.

Price, P. B., Rohde, R. A., and Bay, R. C.: Fluxes of microbes, organic aerosols, dust, sea-salt Na ions, non-sea-salt Ca ions, and methanesulfonate onto Greenland and Antarctic ice, Biogeosciences, 6, 479–486, https://doi.org/10.5194/BG-6-479-2009, 2009.

Procházková, L., Řezanka, T., Nedbalová, L., and Remias, D.: Unicellular versus Filamentous: The Glacial Alga Ancylonema alaskana comb. et stat. nov. and Its Ecophysiological Relatedness to Ancylonema nordenskioeldii (Zygnematophyceae, Streptophyta), Microorg. 2021 Vol 9 Page 1103, 9, 1103, https://doi.org/10.3390/MICROORGANISMS9051103, 2021.

Rassner, S. M. E., Cook, J. M., Mitchell, A. C., Stevens, I. T., Irvine-Fynn, T. D. L., Hodson, A. J., and Edwards, A.: The distinctive weathering crust habitat of a High Arctic glacier comprises discrete microbial micro-habitats, Environ. Microbiol., 26, e16617, https://doi.org/10.1111/1462-2920.16617, 2024.

Riedel, T., Biester, H., and Dittmar, T.: Molecular fractionation of dissolved organic matter with metal salts, Environ. Sci. Technol., 46, 4419–4426, https://doi.org/10.1021/ES203901U/SUPPL_FILE/ES203901U_SI_001.PDF, 2012.

Riedel, T., Zark, M., Vähätalo, A. V., Niggemann, J., Spencer, R. G. M., Hernes, P. J., and Dittmar, T.: Molecular signatures of biogeochemical transformations in dissolved organic matter from ten world rivers, Front. Earth Sci., 4, 85, https://doi.org/10.3389/FEART.2016.00085/BIBTEX, 2016.

Rounce, D. R., Hock, R., Maussion, F., Hugonnet, R., Kochtitzky, W., Huss, M., Berthier, E., Brinkerhoff, D., Compagno, L., Copland, L., Farinotti, D., Menounos, B., and McNabb, R. W.: Global glacier change in the 21st century: Every increase in temperature matters, Science, 379, 78–83, https://doi.org/10.1126/science.abo1324, 2023.

Ryan, J. C., Smith, L. C., Van As, D., Cooley, S. W., Cooper, M. G., Pitcher, L. H., and Hubbard, A.: Greenland Ice Sheet surface melt amplified by snowline migration and bare ice exposure, Sci. Adv., 5, https://doi.org/10.1126/SCIADV.AAV3738/SUPPL_FILE/AAV3738_SM.PDF, 2019.

Savory, J. J., Kaiser, N. K., Mckenna, A. M., Xian, F., Blakney, G. T., Rodgers, R. P., Hendrickson, C. L., and Marshall, A. G.: Measurement Accuracy with a "Walking" Calibration Equation, Anal. Chem., 83, 1732–1736, 2011.

Simonsen, M. F., Baccolo, G., Blunier, T., Borunda, A., Delmonte, B., Frei, R., Goldstein, S., Grinsted, A., Kjær, H. A., Sowers, T., Svensson, A., Vinther, B., Vladimirova, D., Winckler, G., Winstrup, M., and Vallelonga, P.: East Greenland ice core dust record reveals timing of Greenland ice sheet advance and retreat, Nat. Commun., 10, 4494, https://doi.org/10.1038/s41467-019-12546-2, 2019.

Singer, G. A., Fasching, C., Wilhelm, L., Niggemann, J., Steier, P., Dittmar, T., and Battin, T. J.: Biogeochemically diverse organic matter in Alpine glaciers and its downstream fate, Nat. Geosci., 5, 710–714, https://doi.org/10.1038/ngeo1581, 2012.

Smith, D. F., Podgorski, D. C., Rodgers, R. P., Blakney, G. T., and Hendrickson, C. L.: 21 Tesla FT-ICR Mass Spectrometer for Ultrahigh-Resolution Analysis of Complex Organic Mixtures, Anal. Chem., 90, 2041–2047, https://doi.org/10.1021/ACS.ANALCHEM.7B04159/ASSET/IMAGES/MEDIUM/AC-2017-04159Q_0010.GIF, 2018.

Spencer, R. G. M., Stubbins, A., Hernes, P. J., Baker, A., Mopper, K., Aufdenkampe, A. K., Dyda, R. Y., Mwamba, V. L., Mangangu, A. M., Wabakanghanzi, J. N., and Six, J.: Photochemical degradation of dissolved organic matter and dissolved lignin phenols from the Congo River, J. Geophys. Res. Biogeosciences, 114, 3010, https://doi.org/10.1029/2009JG000968, 2009.

Spencer, R. G. M., Guo, W., Raymond, P. A., Dittmar, T., Hood, E., Fellman, J., and Stubbins, A.: Source and biolability of ancient dissolved organic matter in glacier and lake ecosystems on the Tibetan Plateau, Geochim. Cosmochim. Acta, 142, 64–74, https://doi.org/10.1016/J.GCA.2014.08.006, 2014.

Spencer, R. G. M., Mann, P. J., Dittmar, T., Eglinton, T. I., McIntyre, C., Holmes, R. M., Zimov, N., and Stubbins, A.: Detecting the signature of permafrost thaw in Arctic rivers, Geophys. Res. Lett., 42, 2830–2835, https://doi.org/10.1002/2015GL063498, 2015.

Steger, C. R., Reijmer, C. H., and Van Den Broeke, M. R.: The modelled liquid water balance of the Greenland Ice Sheet, Cryosphere, 11, 2507–2526, https://doi.org/10.5194/tc-11-2507-2017, 2017.

Stevens, I. T., Irvine-Fynn, T. D. L., Porter, P. R., Cook, J. M., Edwards, A., Smart, M., Moorman, B. J., Hodson, A. J., and Mitchell, A. C.: Near-surface hydraulic conductivity of northern hemisphere glaciers, Hydrol. Process., 32, 850–865, https://doi.org/10.1002/HYP.11439, 2018.

Stevens, I. T., Irvine-Fynn, T. D. L., Edwards, A., Mitchell, A. C., Cook, J. M., Porter, P. R., Holt, T. O., Huss, M., Fettweis, X., Moorman, B. J., Sattler, B., and Hodson, A. J.: Spatially consistent microbial biomass and future cellular carbon release from melting Northern Hemisphere glacier surfaces, Commun. Earth Environ., 3, 1–10, https://doi.org/10.1038/s43247-022-00609-0, 2022.

Stibal, M., Šabacká, M., and Žárský, J.: Biological processes on glacier and ice sheet surfaces, Nat. Geosci., 5, 771–774, https://doi.org/10.1038/ngeo1611, 2012.

Stubbins, A., Spencer, R. G. M., Chen, H., Hatcher, P. G., Mopper, K., Hernes, P. J., Mwamba, V. L., Mangangu, A. M., Wabakanghanzi, J. N., and Six, J.: Illuminated darkness: Molecular signatures of Congo River dissolved organic matter and its photochemical alteration as revealed by ultrahigh precision mass spectrometry, Limnol. Oceanogr., 55, 1467–1477, https://doi.org/10.4319/LO.2010.55.4.1467, 2010.

Stubbins, A., Hood, E., Raymond, P. A., Aiken, G. R., Sleighter, R. L., Hernes, P. J., Butman, D., Hatcher, P. G., Striegl, R. G., Schuster, P., Abdulla, H. A. N., Vermilyea, A. W., Scott, D. T., and Spencer, R. G. M.: Anthropogenic aerosols as a source of ancient dissolved organic matter in glaciers, Nat. Geosci. 2012 53, 5, 198–201, https://doi.org/10.1038/ngeo1403, 2012.

Yallop, M. L., Anesio, A. M., Perkins, R. G., Cook, J., Telling, J., Fagan, D., MacFarlane, J., Stibal, M., Barker, G., Bellas, C., Hodson, A., Tranter, M., Wadham, J., and Roberts, N. W.: Photophysiology and albedo-changing potential of the ice algal community on the surface of the Greenland ice sheet, ISME J. 2012 612, 6, 2302–2313, https://doi.org/10.1038/ismej.2012.107, 2012.

Yang, K., Smith, L. C., Karlstrom, L., Cooper, M. G., Tedesco, M., van As, D., Cheng, X., Chen, Z., and Li, M.: A new surface meltwater routing model for use on the Greenland Ice Sheet surface, The Cryosphere, 12, 3791–3811, https://doi.org/10.5194/tc-12-3791-2018, 2018.